Journal of Visualization, Vol. 1, No. 3 (1999) 239-253

Radar Imagery : Looking from Space with Wavelengths 100000 Times Larger than the Ones of Visible Light

Massonnet, D.*

* CNES (French Space Agency), 18 Avenue, E. Belin 31401, Toulouse CEDEX4, France.

Received 3 August 1998.
Revised 3 November 1998.

***Abstract*:** Radar instruments are used to observe the Earth with radio waves. The resulting image reflects both the physical properties of the waves and the technological choices that have to be made to obtain a usable image from the raw data gathered by the instrument. We describe the way a radar image is obtained through computer as a two-fold image. The first part, the amplitude, conveys a similar, but different information than conventional imagery, such as the geometry of pixel layout on the ground and the estimation of the speed of mobile targets on land or sea. The second part, the phase, cannot be visualized by itself and gains value only through the comparison with the similar part of a companion image. An accurate description of terrain elevation can be obtained from the slight difference of point of view between the images. A much more accurate assessment of terrain displacement, down to millimeters, between the acquisition dates of the images can also be obtained. In addition, otherwise invisible meteorological phenomena can be mapped. We describe examples of the way these various pieces of information are obtained together or separately, as well as ways to combine the results into a singe color image.

***Keywords*:** remote sensing, radar, interferometry, space geodesy, digital elevation models.

1. Introduction

Radar instruments used to observe the Earth can visualize radically different aspect of nature than optical instruments. The 100000 typical ratio between visible light and radio waves creates major physical differences between the resulting images. To consider the magnitude of the expected difference, it suffices to consider that the ratio of the wavelengths used, on one hand, for a usual identity photograph and, on the other hand, for an X-ray scanning of the skull, is far from being as high. With radio waves, we see mostly the geometric and physical properties of the ground, whereas optical images are more sensitive to the chemical nature of the ground, with wavelengths close to the ones typical of molecular transitions. In other terms, a radar image is sensitive to macroscopic properties, such as moisture (through the induced changes of the electrical conductivity) or large scale geometric features, since the wavelengths of several centimeters are scaled to usual natural or artificial objects. Mirror-like reflections are commonplace in radar imagery, often caused by double specular reflection between right angled objects. Examples include the action of bridge pillars over water, sidewalks or any right-angled structures in cities or tree trunks over flat ground or even water. Specular reflections are rather uncommon in optical imagery and require much better surface smoothness and much sharper orientation. Most of the radio waves are stopped by the ground, or even vegetation, to within a small fraction of the wavelength, if the objects are conducting electricity, a very general case with usual conditions of moisture. However, in hyperarid deserts or in ultra cold environment, such as Arctic and Antarctic where no liquid water can enhance conductivity, a sizable penetration takes place, exceeding several or several tens of wavelengths, and allowing to image subsurface or buried features.

Although this is a way to visualize things that could not be observed otherwise, we will rather concentrate, in this paper, on radar visualization processes resulting from the technological requirements of radar (Wiley, 1985), and first of all by obtaining the image itself, which much be reconstructed by applying heavy computation on instrumental raw data, rather than resulting from a relatively simpler light gathering device. A most useful feature of radar images arises from the transparency of the atmosphere to radar waves, whether clear or loaded with clouds, fog or aerosols. The atmosphere has some effect on the signal (see Subsection 3.5), but does not prevent the wave to reach the ground. Images can also be obtained during night, since the radar instrument is its own source.

2. Constructing Radar Images

2.1 General Principles

The large wavelength used for radar is very beneficial, because the frequency content of the signal is small enough to allow us to record it in amplitude and phase, but it is difficult to manage on a technological point of view because the angular sharpness of any electromagnetic instrument is inversely proportional to its aperture and proportional to the typical wavelength observed. Since wavelengths in the radio range are typically one hundred thousand times that used in an optical image, a similar resolution to that of the human eye would require an aperture of the radar instrument one hundred thousand times larger than the pupil, or about 300 meter just to be able to distinguish the details on the ground an astronaut would make out from the same orbit. In reality, a space

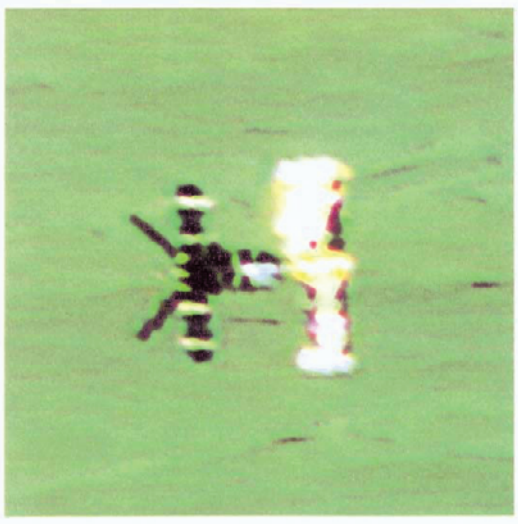

Fig. 1. Typical aspect of a radar satellite : ERS2. The figure is the actual satellite as it is seen by SPOT, a remote sensing satellite using visible light to produce images. SPOT is designed to create images of the ground with a 10-meter resolution, while traveling, with respect to ground, at about 6.7 kilometer-a-second at an altitude of about 820 km. In contrast, ERS2 flies about 780 kilometer above ground. From the laws of orbit mechanics, the speed of ERS2 exceeds the one of SPOT by about 100 meter-a-second with respect to the ground. Given that ERS2 is typically 20 times closer than the usual targets of SPOT, the resolution of its optical instrument is 50 centimeter rather than 10 meter. This would have resulted in the sampling of SPOT being 20 times too slow for a correct sampling of the image of ERS2. However, ERS2 travels typically 67 times more slowly than the ground does. This second effect compensates the first partially, resulting in a slight over sampling of the image, which has been corrected by Philippe Kubik, from CNES, using advanced filtering techniques. At the end the correct aspect of the radar satellite was regained. The precise localization for this strange "image space rendez-vous" was computed by Dominique Forcioli, also from CNES. The radar antenna is the dark structure with stripes. It is ten meter long and oriented along the velocity vector of the satellite, so that it looks to the side of the satellite. The antenna plane does not face the ground, since the radar cannot look vertically in order to apply the principle of sorting by increasing distance. Despite the size of the antenna, the relative aperture (the length divided by the wavelength) is poor, about 200. For the human eye, the relative aperture is about 6000. This physical constraint explains why radar raw data feature a poor resolution, about five kilometers on the ground.

radar antenna such as the one caught in flight in Fig. 1 is typically in the ten meter range. The sharpening of a radar image cannot therefore be based on the resolving power of the radar instrument, but on two complementary principles that contribute to the spectacular improvement in resolution between initial data and processed data (illustrated in Fig. 2). The first, very usual in radar technology, consists in sorting different points on the ground by the time that the radar wave takes to complete the round trip distance (range imaging). The sampling is typically tens of megahertz, which yields separations of about ten meters on the ground. Each sample includes the wave amplitude and phase. The second principle is less straightforward and is called Doppler imagery, or antenna synthesis. It consists in separating the points along the direction of the velocity of the radar carrier through a detailed analysis of the phases of the successive radar signals. In order for these techniques to work together to obtain a well resolved image in the two main directions, the instrument must look to the side (the viewing geometry of a radar is depicted in Fig. 3).

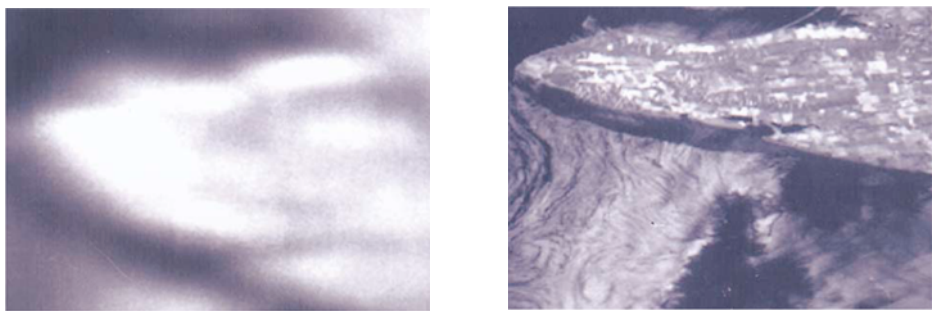

(a) (b)

Fig. 2. Effect of image formation on data. The blurred image (a) represents the amplitude part of the raw signal as delivered by the satellite, before any processing. The sharp image (b) represents the signal after processing. Only the amplitude part is represented (i.e. the module of the complex signal delivered). If represented, the phase of the signal would be noise evenly distributed on a full phase cycle. Surprisingly, although the phase plays a major role in image formation, it remains as noisy in a processed image as it is before processing. Only the comparison of two images can convey a geometric information. The image is a 100 km by 100 km area over Crimea (Ukraine). It has been acquired by the satellite ERS-1 in 1991, and processed in CNES.

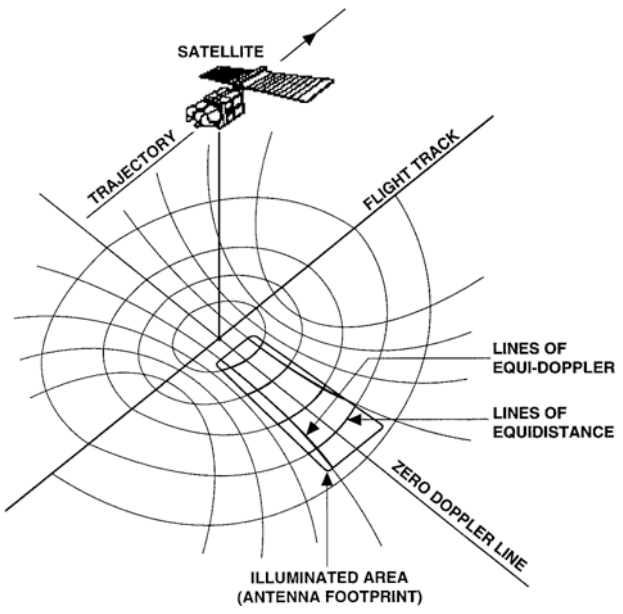

Fig. 3. Viewing geometry of a radar. The instrument takes advantage of the possibility to sort echo samples by distance (closed lines). The synthetic aperture processing allows to distinguish points by their Doppler effect (open lines). If the instrument looks to the side, both principles work together to cut the antenna print into high resolution pixels.

The principle of range imaging creates specific artifacts, which have no equivalent in optics. Depending on the incidence angle of the radar wave, two points (for example the peak of a mountain and the bottom of a valley) can be at the same range from the radar and their contributions will be irremediably mixed together in the same point of the radar image. This is the "overlay" phenomenon, exemplified in Fig. 4.

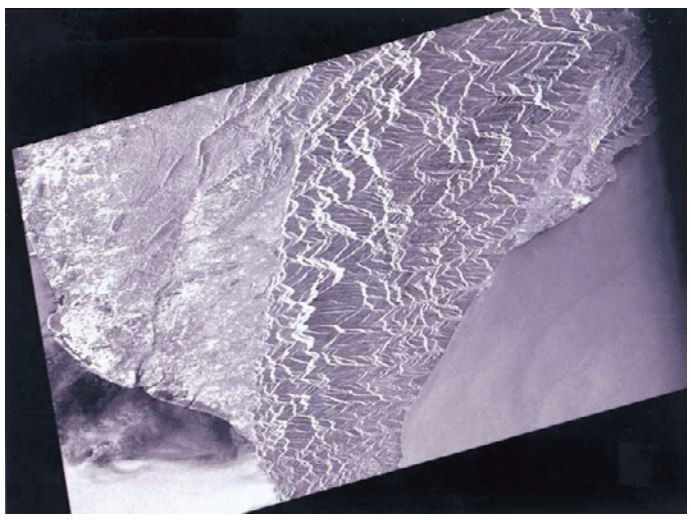

Fig. 4. Difficulties brought by the principle of distance imagery observed on a mountainous area in Taïwan. Distance ordering is compatible with cartographic coordinates over flat terrain. In mountainous areas, it might happen that the slope of the terrain equals the angle of incidence of the radar. In this case, the slope is all contained in a single pixel in distance. If the slope stays below the incidence, we have foreshortening (the slope looks as if "compressed" by the distance perspective). If the slope exceeds the incidence, the top of a mountain is seen closer than its foot. Contributions from points from the summit area and points from the valley are mixed together irreversibly, a phenomenon called layover. This effect has no equivalent in conventional imagery. We are more used to shadowing, where an obstacle such a mountain prevents any signal from returning to the radar. Such a phenomenon can be observed on the other side of the mountain. These data from ERS-1 where obtained from the receiving station in Taiwan and processed at CNES, for the sake of comparing the performances of two interferometric processors, in a cooperative effort with Prof. Cheng.

2.2 Principle of Antenna Synthesis

The principle of antenna synthesis is explained in Fig. 5. A target A will respond to successive pulses emitted by the radar instrument as long as it stays within the antenna footprint L. The size of the footprint is related to the length of the radar antenna D and the distance of observation R by : $\lambda R = DL$, where λ is the wavelength. The number of pulses our target A will contribute to, N, is the ratio of the antenna footprint L and of the distance covered by the satellite between pulse emissions, which we call p, or azimuth pixel size. N is therefore the factor of improvement in resolution that we seek from the processing. In reality, N is on the order of 1000 to 4000 but, in Fig. 5, we have set N to 7 for the sake of clarity. The distance R is typically 1000 km and the antenna footprint typically 5 km wide, so L is much smaller than R. At both ends of target crossing, the radar-target distance will exceed the shortest distance R by a couple of meters typically. Assuming our target A is alone on the ground, the phase of each pulse would vary only in relation to its extra round trip distance compared to 2 R. Each point of the signal is formed by an amplitude and a phase with the latter influenced from pulse to pulse by the variation of range between the target and the radar. This variation of round trip distance can be modeled, so we can manipulate the successive pulses, and namely rotate their phases by computer, in order to have the same phase for each pulse, if they were produced only by our target A. In these conditions, the corrected pulses will add together efficiently. Our target A is not alone, but mixed, in each pulse, with all the targets lying within the antenna footprint L. To understand what happens to these targets through the above processing devoted to A, let us consider again Fig. 5. After having applied the processing devoted to A, the difference with what would have been the ideal processing for B is represented by the red segments. Let us assume that they vary by half a wavelength along L. Once

multiplied by two to account for the round trip travel, the contributions of the target B will describe all the possible residual phase and the addition of the manipulated pulses will eliminate B. The condition for the angle BOA requests that : 2 $pL = \lambda R$. Thus, in conjunction with the aperture condition $DL = \lambda R$, we come to the surprising condition : $2p = D$, saying that the resolution along the track is equal to half the antenna length. The same applies to a target twice as far from A than B is. The phase residuals will simply describe two full phase cycles during analysis and will cancel similarly. This process works as far as a neighbor target does not add one full phase cycle between each pulse, compared to A. In this case, the processing devoted to A is formally equivalent to the ideal processing for this target (ambiguous target C in Fig. 5). The antenna pattern must therefore be such as to keep C outside. We must have : $L <$ [AC] therefore $L < Np$. The improvement of the resolution is paid with the size of the processing. N samples must be fumbled and "phase rotated" to produce a single end-point. From our relations it comes that :

$$N > \frac{2R\lambda}{D2}$$

The quite complicated processing which turns the radar raw data into fully focused data has many more features (Curlander and McDonough, 1991), but does not alter the complex nature of the data, amplitude and phase. Any radar observation is not instantaneous, but extends on the time required for a given target to cross the

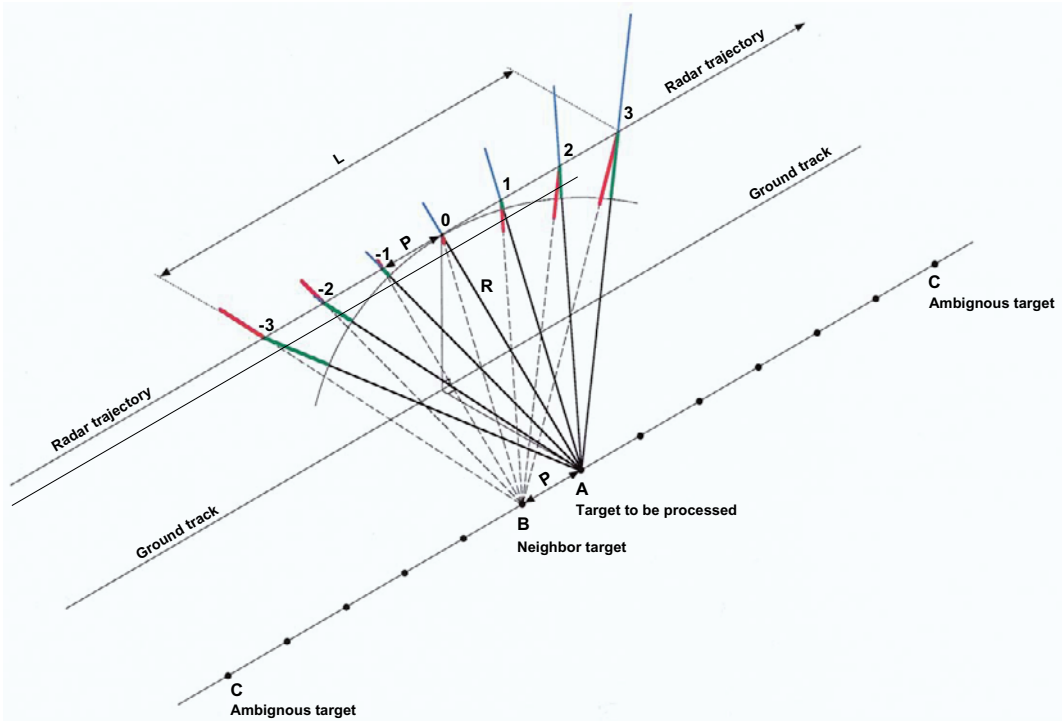

Fig. 5. Principle of Doppler imagery. The distance R represents the closest distance between the radar and the target A. The length during which A is observed (antenna footprint) is L. The optimal processing for A compensates the difference of phase caused by the excess of round trip distance in any pulse emitted along L, with respect to the closest distance, represented by twice the green segments. For the neighbor target B, the previous processing is a disaster : the compensation applied for A results in the residual, red segment, corresponding to an even distribution of phase which differs from optimal B processing by half the wavelength on one end, and minus half the wavelength on the other side (the red segments are indeed at most a quarter of the wavelength at both ends, but this offset is traveled round trip). The contributions of B are jammed all around every value in a phase cycle. The same is true for every target till target C, the "ambiguous target." For this target, the change with respect to A reaches a full cycle between every pulses (or half a wavelength for a single path). The processing for A is as optimal for C, which therefore must lie outside of the antenna footprint. If a target is mobile, it will add a new contribution (the blue segments) to the phase of the signal. Even if the largest of these segments is well smaller than the size of a pixel, it represents easily several wavelengths. As a result, the optimal processing for A, now assumed mobile, will not be the one of a motionless A, but the one of one its neighbor targets, therefore causing the displacement artifact.

antenna footprint, or typically 5 km, or typically less than one second at orbital velocities. From a geometric point of view, with motionless ground targets (unlike the situation of Subsection 2.3), the image is tied to the position of the radar carrier and to its velocity vector and its geometry does not depend on the orientation of the radar, which makes locating it much more precise than for the equivalent optical imagery. This is due to the respective technological performances in pointing and position determination. The amplitude of the image has an unusual appearance because a pixel of the final image is the sum of complex numbers which are representative of the different elementary targets to be found in the pixel. The amplitudes of two identical targets present in the same pixel are added if their phases are identical and cancel each other if the phases are opposite. In reality, many elementary targets lie within each pixel, and the radar amplitude is characterized by an unpleasant scintillation noise ("speckle"). Because of the varied positions of elementary targets within the pixel, and the attached phase rotation, the phase of the image is random spatially, but is deterministic if the configuration of the elementary targets has not changed with time. This allows the comparison of phase values between corresponding points in various radar images or, in other words, radar interferometry (Section 3).

2.3 Velocity Imaging

For moving targets the above mechanism does not work, and, although such targets are correctly focused, they are not placed correctly in the image. In radar images, ships sail off their tracks as we see in Fig. 6. To explain this we must come back to Fig. 5.

If the target A closes to the radar through its own motion, it will create an additional change of phase represented by the blue segments in Fig. 5. As a result, the target A will not be focused by the processing normally devoted to the geometric position of A. To take an example, if the length of the blue segments matches the one of the red segments, the mobile A will be processed by the processing optimal for B !

The explanation behind this deals with ambiguity. We cannot distinguish between phase changes due to radar motion or due to the own motion of the target. We mostly assume a motionless target to lift the ambiguity. In the case of ships, we can lift the ambiguity because we know a ship to be at the end of its wake. Similarly, we know trains run on their tracks and automobiles run on freeways. By adding such new pieces of information, we can lift the ambiguity and come to know the position and the velocity of the target, from its "artificial" displacement.

Fig. 6. In this image from ERS-1 over the British Channel, we observed a spectacular feature of radar imaging : the direct observation of the velocity of a mobile target on the image. The Doppler processing in azimuth assumes motionless ground targets. Even a moderate speed, such as one which does not allow a pixel change during image analysis and synthesis, is sufficient to create a displacement artifact of several hundreds of meters. The phenomenon is due to a position-velocity ambiguity in the processing. In the case of ships, we know the ships must be on their wakes in reality. This external piece of information allows us to naturally lift the intrinsic ambiguity, and to come to know both the position and speed of the ships. Ships are moved along the track of the satellite, in opposite direction depending on whether they close to the satellite or recede from it. The apparent displacement is proportional to the line-of-sight velocity of the ships.

The very specific character of this "velocity imaging" process is attested by the following : assume that A moves toward the radar with a velocity of one meter-a-second. Since the typical time required for target analysis (or, equivalently, antenna footprint crossing) is close to one second, the target A will merely travel one meter, a small fraction of the 10-meter or 20-meter pixel. This means that such a displacement is below the detection threshold of conventional imagery, but this additional meter represents 35 times "half the wavelength". From Fig. 5 we deduce that mobile target A will be processed correctly by the processing matched to its 35th neighbor. With an azimuth pixel size of 5 meter (half the 10 meter antenna length), the target A will be moved by 175 meter from its real position.

3. Combining Radar Images Using the Technique of Interferometry

3.1 General Description

The amplitude of a radar image is more or less the equivalent of what an optical image gives. In contrast, the signal phase indicates at what stage of the wave rotation we are. If the wave travels an integer number of wavelengths, its status will be the same as when it has been emitted. The image of the phase change observed between two radar images is called an interferogram. Such an image potentially records any geometric change between the two images as phase shifts. They take the form of interference fringes, each of which represents a change of geometry of half a radar wavelength between images, hence a full wavelength in round trip. Such fringes are often displayed by full cycles of a color table (Fig. 7 and others). We cannot be sure that the phase is meaningful because any change in the surface observed could also cause random changes in the way the wave is reflected. To ensure that the change of phase is meaningful, neighbor images elements must agree on its value or at least show continuity. This degree of agreement can be measured mathematically and the result is called coherence.

Radar interferometry produces various pieces of geometric information, usually mixed together on the same image such as topographic mapping (Graham, 1974; Zebker and Goldstein, 1986) together with ground displacement mapping. There are also artifact contributions due to changes in the atmosphere during imaging. In

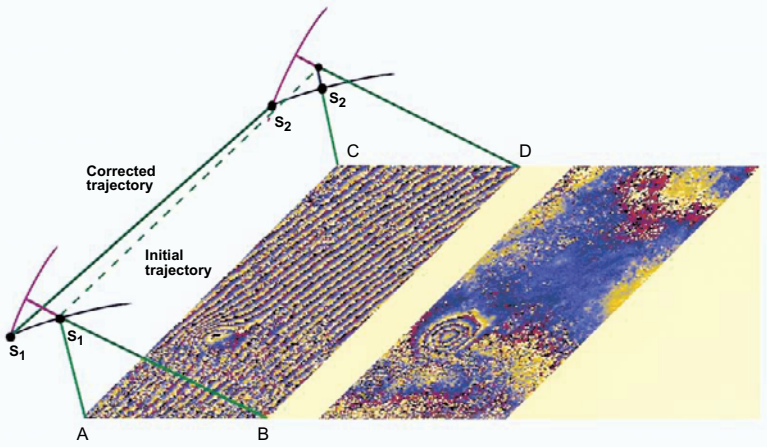

Fig. 7. Visualization of orbital separation between two radar satellites through the analysis of "orbital fringes." We count 15 fringes remaining from point A to B, after correcting from our *a priori* knowledge of the orbits. The distance between the satellite S_1 and B should therefore be lengthened by 15 times half the wavelength, compared to what we thought it was. If the distance between A and B remains unchanged the corrected satellite position can be found where the green and red circles intersect. Keeping A as a reference, we found that distance DS_2 should be lengthened (by 4 cycles) and distance CS_2 shortened (by 10 cycles), which gives the refined position at the end of the interferogram. From this operation we obtain a refined trajectory accurate to, typically, one centimeter or less. This has to be understood as the accuracy of the relative positioning of the two satellite track used. No absolute positioning of the tracks can be obtained by interferometry, an essentially differential technique. The perfect elimination of "orbital fringes" reveals underlying phenomena, such has the deformation field caused by an earthquake (right), which was hardly noticeable before.

order to avoid interpretation errors, one must know how to detect and classify these contributions (Massonnet and Feigl, 1995).

The two images combined into an interferogram will have, in general, different perspectives, since they were not acquired from exactly the same position, and a time difference, since their acquisition dates differ. These two differences almost always occur together in an interferogram and are behind the two types of information provided by interferometry. The difference in perspective creates the topographic information in the interferogram and reveals the orbital difference between the tracks. The difference in time creates information on displacement and is also influenced by the state of the atmosphere during the two image acquisitions.

3.2 Observing Tiny Orbital Shifts

The geometric difference between the two radar images measured as phase changes in an interferogram is dominated by "orbital fringes." The slight difference in the incidence angle between the two images will create a progressive shift from one image to the next. For example, even if this difference only creates a tenth of a phase cycle on a pixel, it will create a full cycle every ten pixels, and several hundreds of cycles over the width of an image. Interference fringes of this type, called "orbital fringes," can be eliminated by computations based on the trajectories. Because of uncertainties in the orbit, some fringes may remain after this correction. These fringes are used to refine the trajectories in the same way that the alignment of mirrors is adjusted in an optical interferometer (see Fig. 7 for the principle of this correction). The orbital fringes also tell us what is the practical limit of orbit separation. We cannot admit a shift close to, or larger than, one fringe per pixel without loosing the ability to identify fringes. This condition places a very strict limit on the satellite tracks, which must be repeated to within one kilometer, typically.

3.3 Production of Elevation Maps

In subtracting the orbital fringes we have to assume a constant elevation of the terrain. In other terms, keeping our previous idea, we have assumed that the mirrors of the interferometer are perfectly flat. If it is not the case, the orbital fringes are distorted by the relief. The latter appears as "fringe contour lines" as soon as orbital fringes have been removed. Although any fringe still represents a half-a-wavelength deformation between images, it is caused by a much larger topographic difference, amounting to tens or hundreds of meters. The reason for it is that the topography is observed from almost the same point of view, that is a difference of up to typically one kilometer

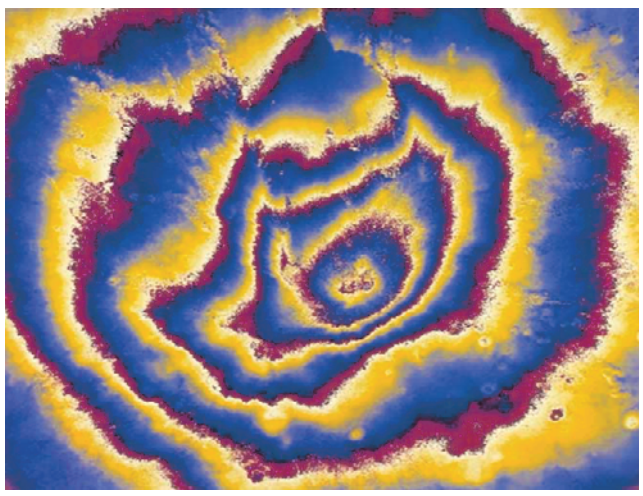

Fig. 8. Example of topographic interferogram obtained on Mount Etna, using data from a radar instrument embarked on the Space Shuttle in 1994 (Sir-C mission). The altitude of ambiguity corresponds about to 500 m. An interferogram is the image of the phase difference between two radar images registered beforehand. Depending on the processing applied, a part or all of the geometric information might have been subtracted from the interferogram. As an example, an interferogram from which the topographic contribution has been subtracted is often called a "differential interferogram." This one had only the orbital fringes removed. The interferometric processing was conducted at CNES using data provided by NASA under the Sir-C investigation program. The interferogram is not registered to a map.

from a typical one thousand kilometer distance. The stereoscopic effect is therefore very small : tens of meters of topography create distorsion of a centimeter or less.

To avoid manipulating complicated geometric equations, it is practical to combine all the parameters involved in the elevation measurement, such as the orbital separation, the wavelength and the incidence angle, in one single significant value, the altitude of ambiguity. This is defined by the variation in elevation that produces a relief fringe. It does not generally vary much on one interferogram and is thus a simple and practical way to characterize one. Figure. 8 shows an example of a topographic interferogram. The altitude of ambiguity decreases as the orbital separation increases. For a radar-carrying satellite such as ERS-1, the altitude of ambiguity can be as low as 10 m before the orbit separation reaches the limit for interferometry.

In mountainous terrain, and after elimination of orbital fringes, an interferogram looks like a family of interference fringes analogous to contour lines, separated in elevation by the local value of the altitude of ambiguity (Fig. 8). The main difference between this interferogram and a topographic map is that the "contour lines" present as fringes are not numbered. Renumbering the fringes, an operation commonly called "phase unwrapping," relies on the continuity of the interferogram. This is what we do when we analyze a topographic map. The noisy areas on the interferogram, as well as the places where the topographic fringes are very close together, pose significant problems to algorithms for automatic unwrapping of fringes, for which many solutions have been proposed (Ghiglia and Romero,1994; Goldstein et al.,1988).

3.4 Production of Displacement Maps

The time difference contributes to the information contained in the interferogram if we assume that orbital and topographic effects have been compensated for. An interferogram can reveal the variations in range linked to the time elapsed between images. Even though these variations may include atmospheric effects, they are mainly useful for measuring ground shifts. If one part of the landscape observed by an image has moved, this displacement will be seen as fringes on the interferogram. Unlike what we have seen for topography, any change in range between the ground and the radar will be recorded as a phase change because it occurs only on one image of the pair. For instance a change in range amounting to half the radar wavelength will show up as a full fringe, or a full color cycle as it is represented. Radar interferometry is thus the ideal tool for visualizing displacements that would be hard to catch as clearly even by placing costly instrumentation on the ground. Interferometry has experienced spectacular developments recently in the measurement of deformations caused by earthquakes

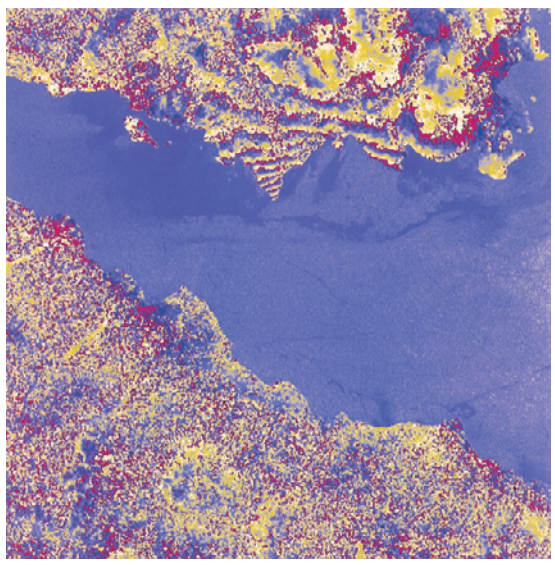

Fig. 9. Example of displacement interferogram obtained on an earthquake in Greece. The ten or so fringes observed in the small cape on the northern coast of the gulf of Corinth result from an earthquake which created a subsidence of about 30 cm (at most). The blue color on the sea surface does not result from interferometric processing, which can only give a pure noise result over water as soon as the two radar images are not acquired simultaneously. It was added by replacing the noisy interferometric signal by the equivalent amplitude from one of the radar images used to form the interferogram, once scaled as to correspond to the blue of the color table.

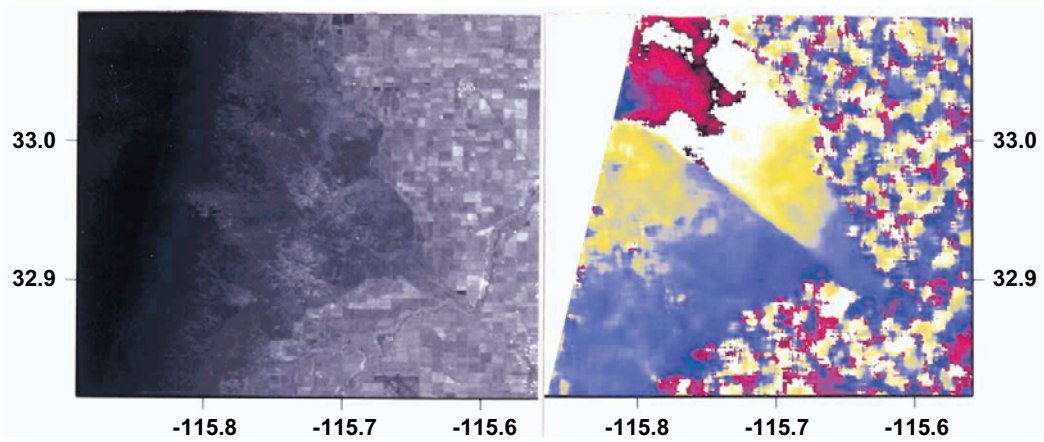

Fig. 10. Example of visualization of a fault slip through interferometry alone. The image on the left is the amplitude of one of the two radar images from ERS-1 used to build the interferogram on the right. Coherence is lost on areas used for agriculture in the two-year-long interferogram. The interferogram covers the same area as the amplitude image, as shown by the latitude and longitude ticks. The fault slip of about 10 mm extends over more than 20 km on superstition hills, as a remote consequence of the Landers earthquake. A full color cycle (i.e. red, white, yellow, blue) represents a deformation amounting to half a radar wavelength, or about 3 cm with the radar of ERS-1. The cut amounts to about one third of it, or 10 mm. The coseismic fault slip has been recognized in the field by R. Sharp in 1992 [EOS, vol. 73, no.43, p.380]. This example illustrates the ability of radar to see tiny phenomena, from very far away, without the help of any ground instrumentation. Such a fault slip is not very obvious as a crack in the tar of a road. Furthermore if, rather than being localized, the fault rupture area is distributed over, say, 20 meter across the fault, it would become extremely difficult to spot on the ground, but would appear with the same clarity in a radar interferogram.

(Massonnet et al., 1993), of which Figure 9 shows an example, glaciers (Goldstein et al., 1993; Mohr et al.,1998); volcanoes (Massonnet et al., 1995), and even phenomena with smaller amplitudes like post-seismic motion (Massonnet et al., 1996; Pelzer et al.,1996) or continental drift (Vadon and Sigmundsson, 1997). In some cases, shifts of a few millimeters were accurately mapped (Fig. 10). In the field of hydrology, interferometry has proved to be capable of measuring the quantity of water pumped by geothermal plants (Massonnet et al., 1997). Irrigation also has a direct effect on the phase (Gabriel et al., 1989), which may come from geometric causes (swelling) or physical ones (change in electrical conductivity). The measurement of displacements suffers the same shortcoming as the measurement of topography : fringes must be renumbered, or "unwrapped," to recover their absolute number(Fig. 9) In addition, the measurement is performed only along the radar line of sight. These drawbacks are far from shadowing the interest of the technique.

3.5 Visualization of Atmospheric Phenomena

Phase changes arise from various causes and must be classified. This can be done by following simple logical laws, if several interferograms are available (Massonnet and Feigl, 1995; Massonnet and Feigl, 1998). The following in particular can be distinguished:

(1) structures tied to the orbital difference: This involves phase change patterns viewed in several interferometric combinations of images, with an amplitude proportional to the topographic sensitivity of the interferometric pairs, which itself is tied to the distance between their orbits. This behavior characterizes the non-compensated or poorly corrected topographic residual.

(2) patterns that depend on a date: This involves phase structures viewed with the same amplitude in several interferometric combinations of images, whenever the acquisition dates of the images that form them include a particular date. This behavior characterizes geophysical events like earthquakes.

(3) atmospheric artifacts: this term includes structures that appear, with the same amplitude, in all the interferometric combinations of a given image. This behavior characterizes heterogeneity in the conditions of atmospheric propagation at the exact moment of image acquisition. Since the responsible image can be identified, the sign of the artifact is known. Artifacts that lengthen the trajectory are attributed to pressure

waves or to turbulence in the troposphere and those that shorten it to local neutralizations in the ionosphere (Massonnet and Feigl, 1995).

This list can be expanded with the physical effect of a homogenous change in the atmosphere : if the electromagnetic depth of the atmosphere changes from a scene to the next while staying homogenous within the scenes, no effect will be observed on a flat terrain. This is because whatever path change experienced from one scene to the next is constant over the observed area. However, if the area comprises a strong topography, the radar waves crossing the atmosphere to the top of a mountain will be less changed than waves crossing the atmosphere all the way down to sea level. The homogenous change in the atmosphere will then look exactly as a topographic residual, but *without being dependent on the orbital separation of the image pair.* So even if atmospheric phenomena cannot prevent the acquisition of radar images, they are actually recorded in them, in a unique way to visualize "atmospheric depth" in high resolution. Figure 11 provides an example of how a thick thunderstorm cloud can affect an interferogram.

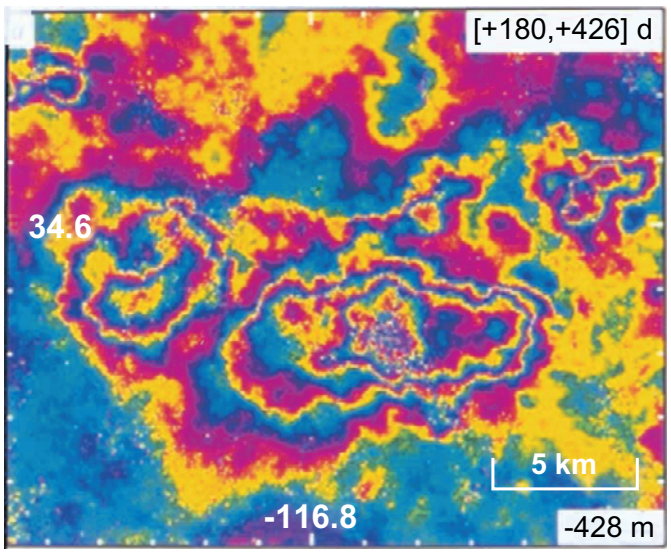

Fig. 11. Example of visualization of meteorological phenomena through radar interferometry. These phenomena are characterized by their insensitivity to the time elapsed between the acquisition of the images used to form the interferogram, as well as their insensitivity to the orbital separation of the corresponding satellite tracks. However, a given radar image is responsible for the same structure observed in several inteferograms with a constant magnitude. Here we see the effect of a heavy atmospheric turbulence caused by a thunderstorm in preparation over the Mojave desert in August 1993 in late afternoon. Having up to four fringes (or 24 cm for ERS-1) or atmospheric two-way delay is exceptional and still unique at this time. The numbers in upper right indicate the dates of acquisition of the two radar images used to form the interferogram, with respect to an arbitrary starting time. The images were separated by 246 days. The number in the lower right gives the topographic sensitivity, close to 250 m per fringe. If the four-fringe feature in the interferogram were uncorrected topography, it should be 1 km deep ! Ticks denote longitude and latitude.

3.6 Representation of Interferograms

One can also use the above characterization of the contents of the interferograms to attenuate or amplify this or that contribution, as exemplified in Fig. 12.

Using integer combination of two different frequencies λ_1 and λ_2 with a ratio close to an integer number n allows a perfect mapping of discontinuous deformation fields provided the amplitude of the deformation, or, more exactly, the amplitude of the discontinuities, remains smaller than the "equivalent" wavelength λ_e :

$$\lambda_e = \frac{1}{\frac{n}{\lambda_1} - \frac{1}{\lambda}}$$

But even with interferograms obtained with the same wavelength, one can eliminate any residual contribution of the topography, for instance. In this case, one must identify any rationale number close to the ratio of topographic sensitivity of two interferograms. The rationale number must be formed with small integers, such as $\pm 1, \pm 2, \pm 3, \pm 4, \pm 5$, in order to avoid multiplying the noise too much. The procedure consists then in multiplying each interferogram by the selected integer factor, and to add the results. In our example, the topographic contribution will be removed almost completely (depending on the resemblance between the real

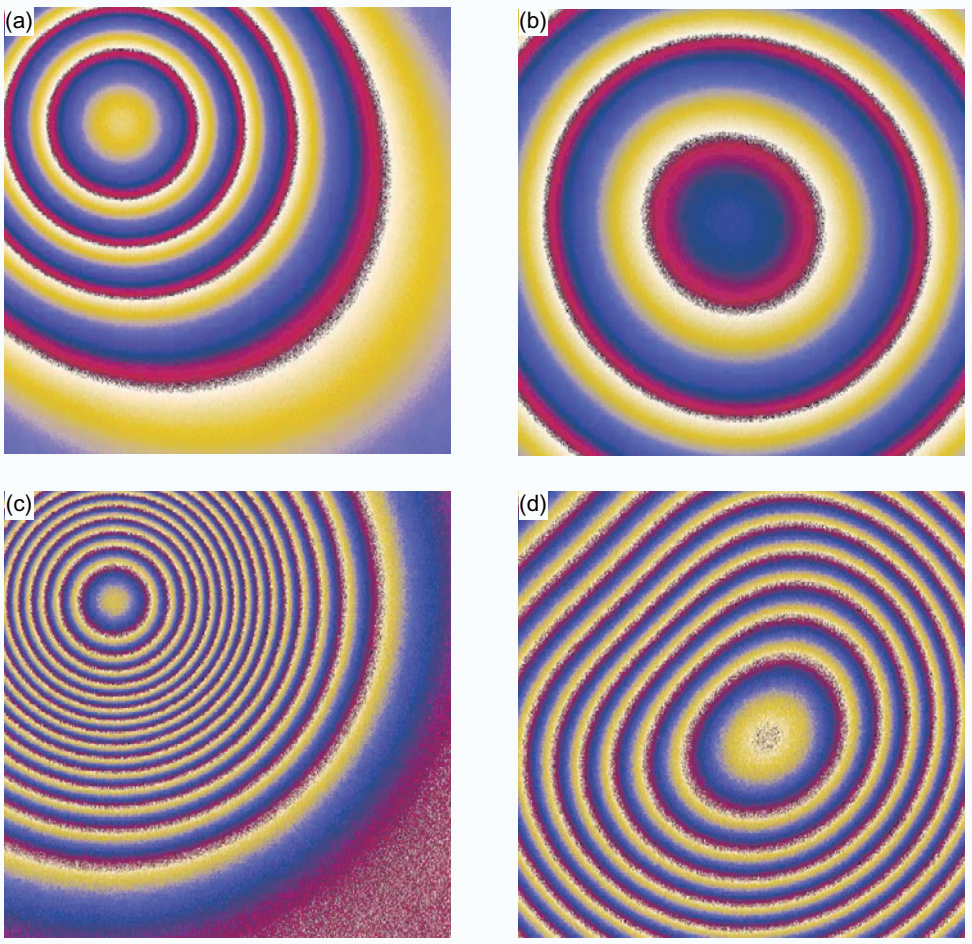

Fig. 12. Example of selective visualization of various effects through physical signatures and integer combination prior to phase unwrapping. In (a) we simulate a C-band (wavelength of 5.656 cm) interferogram with two effects : a circular topographic effect amounting to four fringes and centered in 0.25, 0.25 (taking the side of the image as a unit of length) and a wider, circular ionosphere effect amounting to one fringe, centered on 0.5, 0.5. The second effect is hardly noticeable as a slight distortion of the circular pattern. A likely noise level has been added. In (b), we show the equivalent feature in L-band (wavelength of 23.6 cm). The ratio of the two wavelengths is $R = 4.1732$. Assuming the L and C images have been acquired by the same satellite (a feature of the proposed US-French ECHO/ELSIE mission), the topographic effect will be the same in both interferograms, but will be represented only by $4/R$ fringes in (b) due to the larger wavelength. On the contrary, the ionosphere effect is proportional to the square of the wavelength, and will appear multiplied by R^2 in (b), or multiplied by R in number of fringes. In (b) the topographic effect is hardly noticeable as a distortion. In (c) we took four times the C-band interferogram and subtracted the L-band interferogram, using operations with whole numbers. Due to the multiplication and combinations, the noise climbed somewhat. In (c) the ionosphere contribution became -0.1732 fringes and the topographic contribution became 15.04 fringes, a ratio of 86 ! In (d), we took four times the L-band interferogram and subtracted the C-band interferogram. The ionosphere contribution became 15.69 fringes and the topographic contribution became -0.166 fringes, a ratio of 95 ! This example explains how integer contribution and specific weighting can enhance particular components of the interferometric information, without necessarily unwrapping the interferograms.

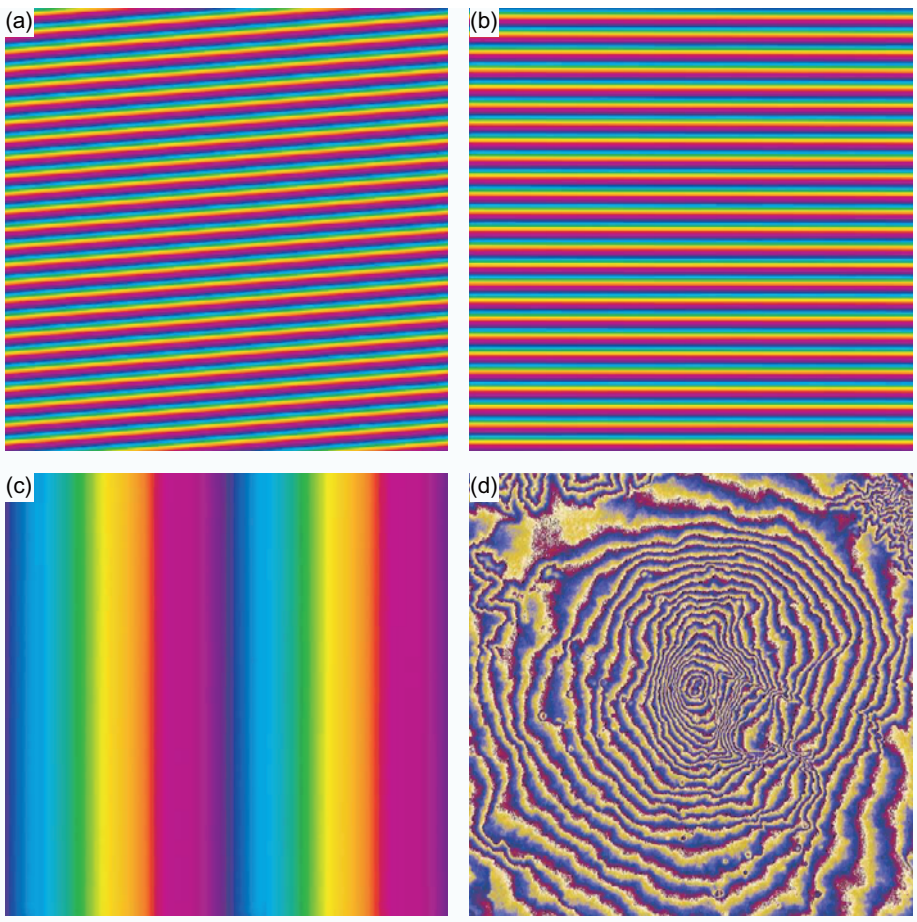

Fig. 13. Examples which contradicts "natural" opinion about fringe behavior. In (a) we have a dense fringe pattern,mostly horizontal. After modeling it with a horizontal fringe pattern of the same density, displayed in (b), we can subtract the modeling and obtain, surprisingly, a purely vertical pattern in (c). Similarly, even ambiguous (i.e. "wrapped") interferograms can be manipulated by linear combination provided they are multiplied by whole numbers. In an ambiguous interferogram, we basically ignore the integer part of the fringes. This part remains an integer if it is multiplied by an integer. In (d), we have a mountain with a topographic sensitivity of 130 meter-per-fringe. In (e), we have a sensitivity of −255 meter-per-fringe. These sensitivities depends on the orbital separation during the acquisition of the two images. Their sign depends on which image is taken as a reference. Simply adding twice (e) to (d) provides an image of the mountain featuring a topographic dependence decreased to −6630 meter-per-fringe seen in (f). In this last image, unwrapping becomes useless because the mountain is not as high as the elevation represented by a single fringe. The combined interferogram (f) can therefore be multiplied by non-integer coefficient in order to automatically unwrap image (d) (the most sensitive to elevation) and to obtain an accurate elevation map.

topographic ratio and the actual rationale number used). The advantage is to avoid the complicated procedure of phase unwrapping, which can occasionally cause large interpretation errors in case of one step of fringe count being missed. Figures 12 and 13 give examples of this procedure which can be applied to topography, the atmospheric residuals, to time dependent geophysical phenomena, all of which being enhanced or attenuated depending on the integer factors used.

Interferograms also create less theoretical problems of representation. The very accurate phase information does not convey the sense of geographic location by itself. The solution is either to put geographic coordinates in the interferogram or to superpose to it another layer of information (the conventional radar image for instance). One can take the opportunity of such a multi-channel representation to correct for the places where fringes are obscured by poor surface preservation between data acquisitions. In Fig. 9, we had somewhat corrected the problem by recognizing surfaces of water (through a geographic file), and replacing the fringes there. In the general case, the interferogram can test itself, by computing coherence which can then be used to map areas where fringes should not be represented. An example is given in Fig. 14, where surfaces covered with vegetation, or surfaces which experienced a fresh lava flow (i.e. poured in between the dates of the radar image acquisitions) cannot be used for interferometry and are left in black and white.

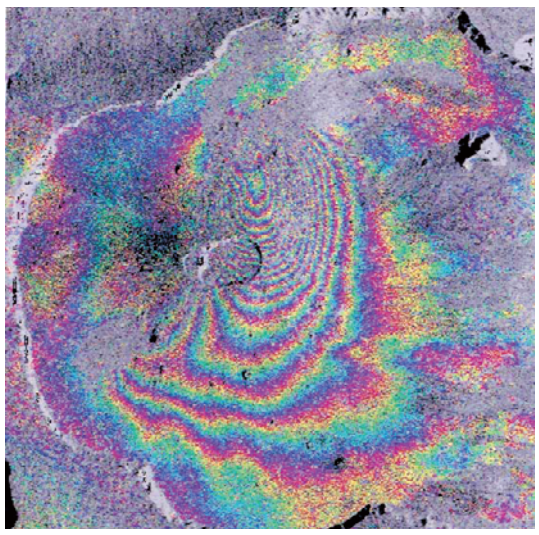

Fig. 14. Example of combination of several level of information through an inverse intensity/hue/saturation transform. In combining phase results and amplitude results, we face two difficulties. First the dynamic range of a radar image is difficult to manipulate, and shows extremely bright and extremely dark areas. Second, fringes do not exist everywhere. What we really want is to reduce the dynamic range to an acceptable level, which can be obtained by taking the logarithm of the image properly scaled. The resulting image is considered as an *intensity* image. We then want to color the image with the fringes. A full color cycle of phase represents some 28 millimeter of displacement along the radar line of sight. An accuracy of 1.5 millimeter would already be an excellent result. Therefore the color is kept on 16 levels only, in order to avoid representing non-significant signal. Color is taken as *hue*. Furthermore, due to "time degradation," the fringes have a varying quality. The coherence, which measures the level of agreement between neighbor pixels, is a good indicator of fringe quality. Taking this indicator, once properly scaled, as *saturation*, makes the resulting image very trustworthy : color (i.e. fringes) appears only where fringe quality is high. An inverse transform turns the combination image into conventional Red, Green, Blue channels. The image represents the deformation caused by a dike injection (a wall-like magma intrusion) north to the main volcanic cone of Mount Piton de La Fournaise, in La R éunion island, Indian Ocean, during its last eruption which started in March 1998. The images from the Canadian satellite RADARSAT have been obtained through an investigation program. The size of one side of the square image is 9 km. The 17 fringes correspond to a line-of-sight displacement of about 50 cm at most (Sigmundsson et al.,1998).

4. Conclusion

Radar imaging is appealing to the visualization technique by many aspects. Just to visualize a radar image is already a challenge which call for a relatively heavy mathematical reconstruction. Even if we put aside spectacular properties linked to the physics of the waves, like the penetration of light vegetation cover or of arid soils, radar images are unique to observe phenomena like the velocity of ground targets or, through the interferometric technique, the turbulence of the atmosphere, the topography of the terrain or small crustal displacements.

The representation of interferograms requires special care. It can be enhanced by a class of image manipulation : the integer combination of interferograms. These manipulations allow to insist on such or such part of the interferometric information at no processing cost. The representation of interferograms together with a conventional image is possible using inverse intensity-hue-saturation transform, in which the color intensity is controlled by the coherence, that is the amount of reliability of the interferometric signal.

References

Curlander, J. C. and McDonough, R. N., Synthetic Aperture Radar: Systems and Signal Processing, (1991) Wiley.

Gabriel, A. K., Goldstein, R. M. and Zebker, H. A., Mapping Small Elevation Changes over Large Areas: Differential Radar Interf erometry, J. Geophys. Res., 94 (1989) 9183-9191.

Ghiglia, D. and Romero L., Robust 2D Weighted Unwrapping that uses Fast Transforms and Iterative Methods, J. Opt. Soc. Am., 11 (1994) 107.

Goldstein, R. M., Zebker, H. A. and Werner, C. L., Satellite Radar Interferometry : Two Dimensional Phase Unwrapping, Radio Sci ence, 23 no. 4(1988)713-720.

Goldstein, R. M., Engelhardt, H., Kamb, B., and Frolich, R. M., Satellite Radar Interferometry for Monitoring Ice Sheet Motion: Application to an Antartic Ice Stream, Science, 262 (1993) 1525-1530.

Graham, L. C., Synthetic Interferometer Radar for Topographic Mapping, Proc. IEEE, 62, 6 (1974) 763-768.

Massonnet, D., Rossi, M. , Carmona, C., Adragna, F. , Peltzer, G. , Feigl, K. and Rabaute, Th., The Displacement Field of the L anders Earthquake mapped by Radar Interferometry, Nature, 364 (1993) 138-142.

Massonnet, D., Briole, P. and Arnaud, A., Deflation of Mount Etna Monitored by Spaceborne Radar Interferometry, Nature, 375 (19 95) 567-570, 1995

Massonnet, D. and Feigl, K.L., Discrimination of Geophysical Phenomena in Satellite Radar Interferograms, Geophys. Res. Lett., 22(12) (1995) 1537-1540.

Massonnet, D., Thatcher,W. and Vadon, H., Detection of Postseismic Fault Zone Collapse following the Landers Earthquake, Nature , 382 (1990) 612-616.

Massonnet, D., Holzer, T. and Vadon, H., Land Subsidence caused by the East Mesa Geothermal Field, California, observed using S AR Interferometry, Geophys. Res. Lett., 24(8) (1997) 901-904.

Massonnet, D. and Feigl, K. L. Radar Interferometry and its Application to Changes in the Earth's Surface, Reviews of geophysic s, 36 (1998) 401-460.

Mohr, J J., Reeh, N. and Madsen, SN. Madsen, Three Dimensional Glacial Flow and Surface Elevation Measured, Nature, 391 (1998) 273.

Peltzer, G., Rosen, P., Rogez, F. and Hudnut, K., Postseismic Rebound in Fault Step-overs caused by Pore Fluid Flow, Science, 2 73 (1996) 1202-1204.

Sigmundsson, F., Durand, Ph. and Manssonet, D., Opening of an Eruptive Fissure and Seaward Displacement at Piton de la Fournais e Volcano Measured by RADARSAT Satellite Radar Interferometry, Geophys. Res. Lett., (submitted 1998)

Vadon, H.and Sigmundsson, F., Crustal Deformation from 1992 to 1995 at the Mid-Atlatic Ridge, southwest Iceland, Mapped by Sate llite Radar Interferometry, Science, 275 (1997) 193-197.

Wiley, C., Synthetic Aperture Radars : A Paradigm for Technology Evolution, IEEE Transactions on Aerospace and Electronic Syste ms, 21-3 (1985) 440-443.

Zebker, H. and Goldstein, R., Topographic Mapping from Interferometric SAR Observations, J. Geophys. Res., 91 (1986) 4993-5001.

Author's Profile

Didier Massonnet: He was born in 1957 and received the B.S. degree from the Ecole Polytechnique, Paris, France in 1982 and from the Ecole Nationale Supérieure des Techniques Avancées (Engineering School for Advanced Studies) in 1984. He obtained a Ph.D. of habilitation from the University of Toulouse in 1997.

He joined CNES (French Space Agency) in 1984 to work in the field of Synthetic Aperture Radar where he developed radar image formation algorithms and performed image quality tests on most airborne and spaceborne radar imaging systems. Radar interferometry was one of his major axes of research. He is now in charge of Research and Development in the Image Processing Division of CNES, in Toulouse, France.

He was awarded the Landucci Prize by the French Academy of Science in 1994 and received the Silver Medal from the Air and Space National Academy in 1998.